

Dynamics of Sheared Ellipses and Circular Disks: Effects of Particle Shape

Somayeh Farhadi and Robert P. Behringer¹

¹*Department of Physics and Center for Nonlinear and Complex Systems,
Box 90305, Duke University, Durham, NC 27708*

(Dated: July 2, 2021)

Much recent effort has focused on glassy and jamming properties of spherical particles. Very little is known about such phenomena for non-spherical particles, and we take a first step by studying ellipses. We find important differences between the dynamical and structural properties of disks and two-dimensional ellipses subject to continuous Couette shear. In particular, ellipses show slow dynamical evolution, without a counterpart in disks, in the mean velocity, local density, orientational order, and local stress. Starting from an unjammed state, ellipses can first jam under shear, and then slowly unjam. The slow unjamming process is understood as a result of gradual changes in their orientations, leading to a denser packing. For disks, the rotation of particles only contributes to relaxation of frictional forces, and hence, does not significantly cause structural changes. For the shear-jammed states, the global building up and relaxation of stress, which occurs in the form of stress avalanches, is qualitatively different for disks and ellipses, and is manifested by different forms of rate-dependence for ellipses vs. disks. Unlike the weak rate dependence typical for many granular systems, ellipses show power-law dependence on the shearing rate, Ω .

PACS numbers: 83.80.Fg , 83.85.St , 83.60.Rs

There has been recent interest in glassy dynamics, jamming[1–3] and rheology[4–10] of particulate systems, such as colloids, emulsions, foams and granular materials. Despite variations in interaction details, particulate systems show similar rheology [11]. Traditionally, rheology concerns aging, rate effects, shear band formation, and failure [7–14]. And, steadily sheared systems provide an alternative route for approaching the jamming transition for particulate systems by moving along the yield stress curve which separates static (jammed) and flowing (unjammed) states in a parameter space of shear stress, τ , and packing fraction, ϕ .

Many recent rheology studies involved spherically symmetric particles. The question we pose is, how does breaking of spherical particle symmetry change the rheology of near-jamming granular materials. A complete answer to this question is beyond the scope of a single paper. Here, we take a first step towards understanding the role played by particle shape by considering elliptical particles. We show that steadily sheared elliptical particles show dramatically stronger rate dependence than their circular counterparts. This rate dependence appears to be linked to slow evolution of the particle orientation. Although we have focused on ellipses because they are easy to characterize, there are key aspects that ellipses share with more complex particle shapes: particle orientation and rotation couple to density and normal contact forces between particles lead to torques.

The ability of particles to exert torques on each other impacts jamming in important ways. For the torque-free case of frictionless spheres, previous simulations[1] reported a fraction, ϕ_J , below which the system is always stress-free (both the pressure, P and τ vanish), and the shear modulus vanishes. Above ϕ_J , there exist $\tau = 0$, $P > 0$ mechanically stable states. In the

frictionless spherical case, if $\phi < \phi_J$, $\dot{\gamma}$ must be non-zero to obtain non-zero τ . However, Bi et al.[3] recently showed that systems of frictional disks behave differently. There exists a range $\phi_S \leq \phi \leq \phi_J$ where it is possible to shear jam a system at fixed ϕ by applying shear strain, starting from a $\tau = P = 0$ state, and arriving at a jammed (mechanically stable) state. Here, ϕ_J corresponds to the lowest density at which frictional granular systems can be jammed at zero τ , and ϕ_S corresponds to the lowest density at which it is possible to jam a system by applying shear strain. These observations are consistent with simulations along the yield stress curve by Otsuki and Hayakawa[15], and older experiments by Howell et al.[6] who observed a what is now understood as a lower limit for shear jamming $\phi_S \simeq 0.76$ for bi-disperse frictional disks subject to Couette shear. Thus, quasi-static shear of frictional spheres (disks in 2D) in the range $\phi_S \leq \phi \leq \phi_J$ is clearly affected by the possibility of shear jamming due to the presence of rotational degrees of freedom. However, for non-spherical particles, such as ellipses, rotational modes are imposed by the geometry even for the frictionless case. This experimental study directly probes the effect of particle asphericity on shear jamming of particulate systems.

A key issue for rheology is the dependence of the shear stress and other properties of a shear system in the strain rate, $\dot{\gamma}$. Here, we contrast two particular cases: a Newtonian fluid has $\tau \propto \dot{\gamma}$, and an ideal granular material has τ independent of $\dot{\gamma}$ for very slow $\dot{\gamma}$ [16]. Although rate-independence for stresses in slowly sheared granular materials has frequently been assumed, there are multiple granular experiments[9, 14, 17] showing logarithmic rate dependence in $\dot{\gamma}$. The true origin of this rate dependence is still an open question, although several groups have proposed models in the spirit of soft glassy

rheology[9, 17]. However, as with many (although not all[18, 19]) studies of jamming, previous work on rate dependence, has typically involved systems of spherical or circular particles, in 3D or 2D, respectively. Here, we show that elliptical particles under sustained shear show stronger rate dependence than their circular counterparts. By inference, this rate dependence is linked to particle orientation.

Here, we directly compare sheared systems of ellipses and of bidisperse disks, and find several crucial differences: 1) Very long transients for P of ellipses but not for disks; there is a packing fraction range for ellipses where P builds up relatively quickly, and then relaxes very slowly. For disks, only monotonic evolution occurs. 2) The order parameter, the density, and the velocity profile exhibit very slow evolution for the ellipse systems; 3) The power spectrum of stress fluctuations for ellipses suggests power-law scaling with rate, with an exponent of $\sim 1/2$; spectra for disks have much weaker rate-dependence.

Experiment: The experimental data of this study were collected from a quasi-2D Couette experiment[6]. This geometry allows continuous shear for arbitrary time/strain intervals. Using this feature, we performed shearing experiments for up to 20 revolutions of the inner wheel, and collected two types of data. In one case, we kept the shear rate constant at $\Omega = 0.01\text{rpm}$, and varied the global packing fraction, ϕ . In the second case, focused on rate dependence, we varied the Ω over a bit more than a decade, for representative packing fractions. All the packing fractions were below ϕ_J , which is 0.84 for disks, and 0.91 for ellipses [24]. Fig.1 gives schematics of the experimental setup. The particles, rest on a smooth horizontal Plexiglas sheet, and are confined between an inner wheel and a rigid, concentric, outer ring. They are continuously sheared by slowly rotating the inner wheel at constant rates, spanning $0.008 \leq \Omega \leq 0.128\text{rpm}$. Both ellipses and disks are made from the same photoelastic material (Vishay polymer PSM-4), and are machined with similar procedures. Thus, the particle surfaces have similar friction coefficients. The ellipses have semi-minor axis $b \simeq 0.25\text{cm}$ and aspect ratio ~ 2 . The radius of the small/large disks is $r_s \simeq 0.38\text{ cm}/r_l \simeq 0.44\text{ cm}$. The number ratio of small-to-large disks is kept at $\sim 9 : 2$. The radii of the inner and outer rings of the Couette apparatus are 10.5 cm and 25 cm respectively. As the system was sheared, two synchronized cameras obtained polarized and unpolarized digital images every $\sim 10\text{s}$. We studied systems of either identical ellipses or bi-disperse collections of disks, for packing fractions near the shear-jammed regime. The unpolarized images yield the centers, and orientations (for ellipses) for each particle; the polarized images provide the local P at the scale of a particle using a measure, g^2 , which is the average gradient square of the photoelastic image intensity, integrated over a particle; g^2 is proportional to local pressure[6, 12].

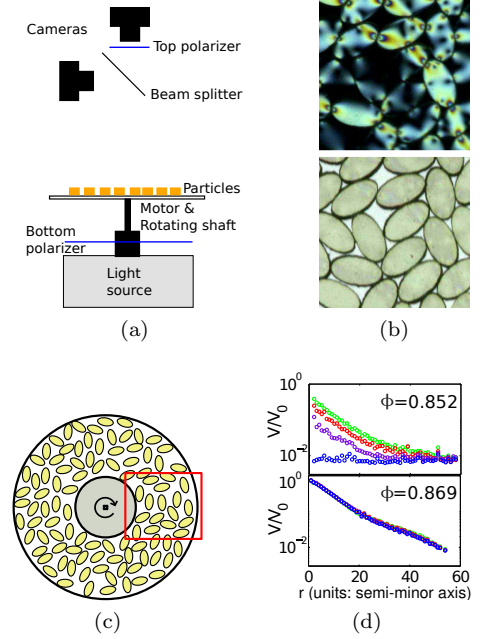


FIG. 1: Schematics of the experimental setup. a) Side view. b) Small segments of polarized/unpolarized images. c) Top view of Couette cell. The inner wheel is lined with small teeth to increase the friction between the wheel and the particles. Circularly polarized light passes through the particles from below, and a beam splitter above the experiment to produce two views of the same region of the experiment, each imaged by a different camera, with and without a (crossed) circular polarizer (relative to the original light polarization). Camera 1 records the particle photoelastic response, providing local stress information of the system[22]; camera 2 yields a direct image of the particles[23]. d) Radial profile of time-average velocities for two representative systems of ellipses. Colors represent the time interval (green:0-5, red:5-10, purple:10-15, and blue:15-20 revolutions). $\Omega = 0.01\text{ rpm}$ for all data.

We used the green channel of our images to compute g^2 , since the photoelastic response is color-dependent, and the polarizers are optimized for green.

We focus on several key results: 1) Anomalous slow relaxation for the motion of ellipses at densities just below the shear-jamming threshold; 2) Differences in the density profiles of disks and ellipses; 3) Slow evolution of the average orientation of ellipses; and 4) Strong, and previously unreported (to our knowledge) rate dependence for stress fluctuations with ellipses that has not counterpart for disks. The first three of these are clearly linked.

Velocities: We show the evolution of velocity profiles for ellipses at two typical ϕ 's in Fig.1(d). The velocity profile is stable for denser states, but for slightly lower ϕ , it relaxes slowly to zero. To quantify the evolution of flow profile, we use the average speed, $V_{int} = \frac{1}{A} \int \langle V \rangle r dr / \int r dr$, where, V is the scalar value of the particle velocity vector, $V = |\vec{v}|$, and A is the area of the

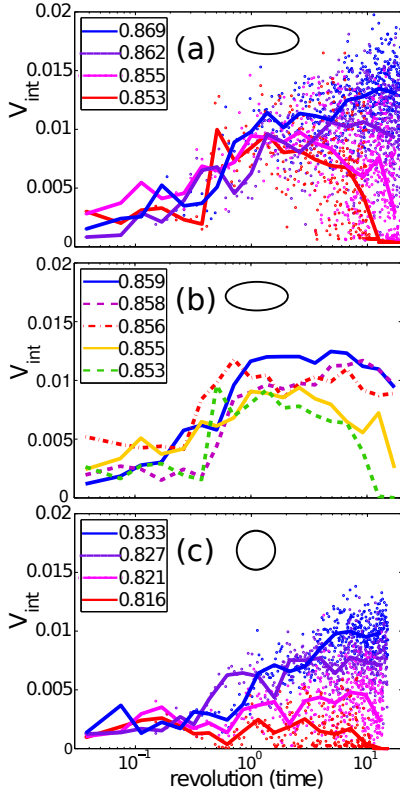


FIG. 2: Evolution of V_{int} for systems of a) ellipses, b) ellipses with ϕ 's corresponding to meta-stable range, c) disks. The legends show global packing fractions. Data points demonstrate V_{int} , sampled from equal time intervals. The lines show the trend of mean value of V_{int} , averaged over logarithmically equal time intervals.

Couette cell. Here, we first focus on a small range of ϕ where transient behavior occurs for ellipses but not for disks. Fig. 2 shows the evolution of V_{int} for ellipses and disks. For ellipses, within a small but non-zero range of 'meta-stable' ϕ 's, V_{int} rises relatively quickly during the first revolution to $V_{int} \simeq 0.01$ for all packing fractions, but then drops slowly to zero. For disks, we found no such meta-stable regime: V_{int} has an almost monotonic trend in the logarithmic time of an experiment. We show the changes in the meta-stable state region in a narrow range of densities, $0.85 \lesssim \phi \lesssim 0.86$, in Fig. 2b. In this, and other figures throughout the paper, systematic errors are at or below the scale of dots used to indicate data points. The apparent noise on the data is due to statistical fluctuations, not to measurement errors.

Structure: local density and orientational order: The gradual decrease in V_{int} for the meta-stable regime of ellipses is associated with a gradual, and anomalously large, increase in Reynolds dilatancy in the region close to the inner wheel, which is facilitated by the evolution of the ellipse orientation. We measure the local density by determining the Voronoi areas, V^v , for individual particles [24]. We take the Voronoi area for a given parti-

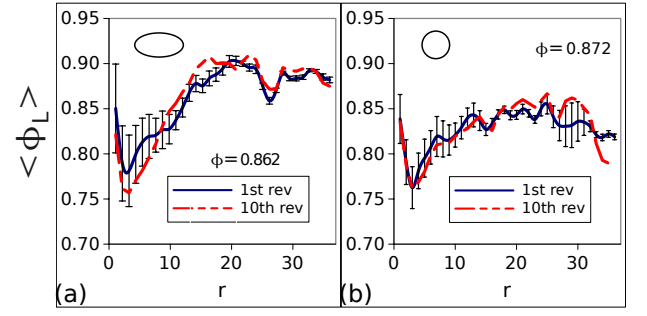


FIG. 3: Radial profiles of time-averaged local densities for ellipses, and disks. r (units: radius of large disk), is the radial distance from the inner wheel's perimeter.

cle to correspond to the interior area of the particle, plus the area corresponding to all points in the plane that are closer to the boundary of the given particle than to the boundary of any other particle. The local solid fraction in the region enclosed by V^v is $\phi_L = \frac{V_0}{V^v}$, where V_0 is the area of a particle. Fig. 3 shows radially and time averaged local density profiles extracted from Voronoi analysis. Close to the inner wheel, both types of particles show a dip in density, i.e. a shear band. Also, the drop in density is roughly twice as big for ellipses (e.g. as a fraction of the mean packing fraction) as for the disks. The small rise in ϕ at the inner wheel is due to the carrying of particles by inner shearing wheel. Since the global packing fraction is fixed for each data set, the relative density minimum near the inner wheel induces closer packing in the middle and outer radial regions of the Couette cell. For all measurements of structure, e.g. for Figs. 2- 5, we keep the rotation rate of the inner wheel fixed at $\Omega = 0.01\text{rpm}$. At the end of this paper, we consider the effects of varying the rotation rate.

It is known that random packing of ellipses can be denser than random disks [19]. However, compacting a randomly prepared system of ellipses requires reorientation of the particles which leads to locally nematic order, as characterized by the local mean *director*. The director has a similar sense as for the liquid crystal context. In order to quantify nematic ordering, we determine the local order parameter q_L . Here, q_L is computed from the orientational order matrix, Q , calculated for small patches of $N \simeq 10$ ellipses surrounding the i 'th particle: $Q_{xy} = \frac{1}{N} \sum_n (u_x^n u_y^n - \frac{1}{2} \delta^{xy})$ [21]. The size of a patch was chosen to give a local average. Here, x and y are two given orthogonal directions, and u^n is the unit vector in the direction of the major axis for a given particle. The summation is made over all particles in the patch. We determine q_L as the maximum eigenvalue of Q .

Fig 4a shows the evolution of $\langle q_L \rangle^*$, the spatially average of q_L , for the outer region of the cell vs. rotations of the inner wheel (on a logarithmic scale). Specifically, we average q_L over a radial region $16a \leq r \leq R_o$, where a is the semi-minor axis of the ellipses and R_o is the radius

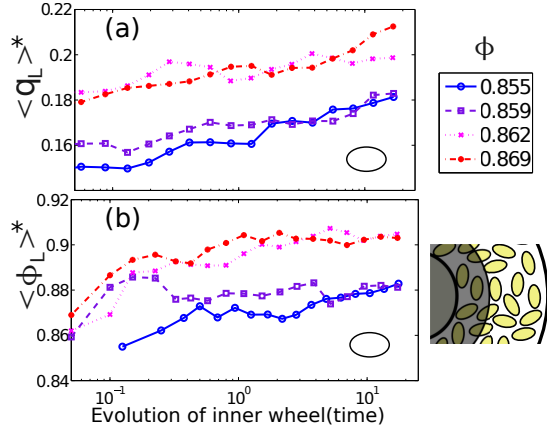


FIG. 4: Evolution of $\langle q_L \rangle^*$ and $\langle \phi_L \rangle^*$ for various packing fractions (legend). $\langle q \rangle^*$ represents the average local orientational order parameter for the area shown as unshaded in schematics shown in lower right, The excluded region is about $16\times$ semi-minor from the inner wheel surface, i.e. roughly the radial width of the shear band.

of the outer confining ring of the Couette cell. In this region, the average velocity is about 10% of the average velocity next to the inner wheel. Considering only this region enables us to characterize the orientational ordering of particles which are almost stationary, but at the same time are reoriented gradually by the dynamics generated in the shear band. In Fig 4a, for all densities, including stable and meta-stable values, $\langle q_L \rangle^*$ increases gradually in time, roughly as $\log(t)$. The evolution of average local densities (from Voronoi analysis) in the same outer region, $\langle \phi_L \rangle^*$, is shown in Fig 4b. Both density and orientational order increase with time, although the relation between these two may not be strictly linear. This extremely slow reorientation and compaction is driven by/allows more dilation in the inner layers. It is then the source of the meta-stability and it subsequently halts the shearing when the compaction in the outer region leads to too weak mechanical contact between the shearing wheel and the ellipses.

Evolution of average pressure: Fig. 5 shows the evolution of the system-average of g^2 for representative packing fractions of disks and ellipses. As mentioned, g^2 quantifies global pressure. For disks, $\langle g^2 \rangle$ attains its initial value relatively quickly in most cases, except for a slight increase over the course of an experiment. However, for ellipses, $\langle g^2 \rangle$ steadily increases over a span of about 10 revolutions of the inner wheel. After this long initial increase, the average g^2 drops only for meta-stable systems and saturates for densities above this range.

Rate dependence of pressure fluctuations: Perhaps the most significant difference in rate effects for ellipses vs. disks occurs for time fluctuations of the pressure in the stable regime. Specifically, the instantaneous pressure of the system is proportional to g^2 integrated over the

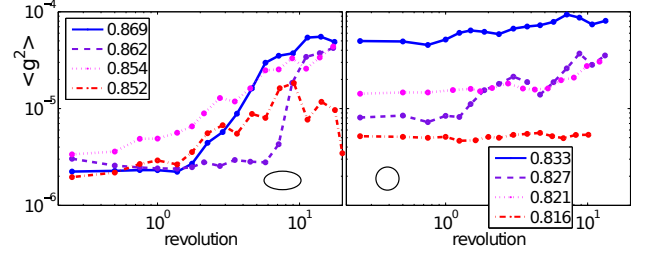


FIG. 5: Evolution of $\langle g^2 \rangle$ for a) ellipses, and b) disks. Legends value indicate the global packing fraction for each data set.

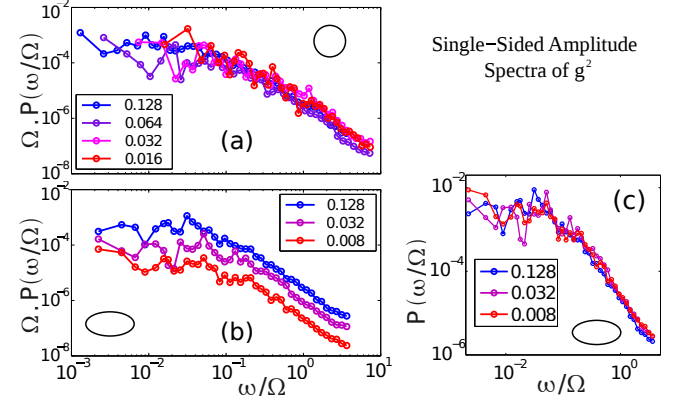


FIG. 6: Scaled power spectral density (PSD) of g^2 for different shear rates, Ω , for systems of: a) disks with $\phi = 0.83$, and b) ellipses with $\phi = 0.86$. c) Here, vertical axis of part b (ellipses) is rescaled by Ω . Note that these data are taken for packing fractions in the stable region, where the velocity profile persists for very large strains (see Fig.1d). The legends indicate the value of Ω in rpm for each data set.

whole field of view. Here, we consider the fluctuations, $\delta g^2(t)$, in time-series of this global $g^2(t)$. Up to this point, the shear rate was held fixed at $\Omega = 0.01\text{rpm}$. Now, we consider the effect of changing Ω , by allowing this quantity to vary over $0.008 \leq \Omega \leq 0.128\text{rpm}$.

The concept of rate-independence is based on the fact that if the strains are slow enough, the system remains very close to a sequence of states in mechanical equilibrium. Then, the system response, for instance the pressure, would depend on the strain, but not the rate of strain, $\dot{\gamma}$. By contrast, if $\dot{\gamma}$ were too high, the system would be out of mechanical equilibrium, and the response would explicitly depend on $\dot{\gamma}$ (here, Ω). The power spectrum, $P(\omega)$, for fluctuations of $g^2(t)$ provide a simple test of whether the system is rate independent or not. Normally, $P(\omega) = T^{-1} |\int_0^T \delta g^2(t) \exp(-i\omega t) dt|^2$, where T is the time over which $\delta g^2(t) = g^2(t) - \langle g^2 \rangle_t$ is measured, and ω is the spectral frequency. If the fluctuations were statistically rate independent, then it would be possible to replace time, t , with strain, $\gamma = \dot{\gamma}t$, or here, Ω . We would then find the same power spectra regardless of

Ω for spectra computed with strain as the variable, instead of time, as discussed for instance by Miller et al.[7]. A straight forward change of variables from t to $\gamma = \dot{\gamma}t$ shows that for the rate independent case, $\Omega P(\omega/\Omega)$ is a function only of ω/Ω . Fig.6a,b show the scaled power spectra computed from $g^2(t)$ for various Ω , where for all cases, the data pertain to stable states. The spectra collapse reasonably well to one generic curve in systems of bi-disperse disks. Hence, the fluctuations of global stress for disks are nearly invariant under changes of shear rate over the range of Ω studied here. (Note that this does not exclude the possibility of weak, e.g. logarithmic rate effects.) These results for disks are qualitatively similar to observations by Miller et al.[7] for fluctuations for systems of sheared 3D spheres. By contrast, similar data for systems of ellipses (Fig.6b) show no collapse, which implies a strong rate dependence. In particular, we observe that the shift in scaled spectra is proportional to the shear rate Ω , Fig.6c. The data suggest that the *fluctuations* in pressure, δg^2 , have a form that is roughly $\delta g^2(t) = \dot{\gamma}^{1/2} f(\dot{\gamma}t)$. This means δg^2 consists of a rate independent term ($f(\dot{\gamma}t)$), times the square root of the shear rate. That is, there is explicit non-trivial rate dependence, which is neither viscous, nor quasi-static. We note that this is a dynamical effect, and to our knowledge, it has not been previously reported.

Conclusions: We have shown through parallel studies using elliptical and circular quasi-2D particles that the long-term rheological behavior of 2D shear jammed granular systems depends significantly on particle shape. The difference in response of ellipses and disks takes several forms, which depend on density. One difference involves transient dynamics in a narrow range of densities, where ellipses show ‘meta-stable’ dynamics that eventually lead to zero-stress states. The velocity, e.g. V_{int} , and the pressure grow to a maxima, and then decay slowly to 0, over large strains, as the particles reorient and compact in the nearly static regions. For densities above the meta-stable regime, the radial profile of ϕ shows a significant minimum for ellipses. The density dip in the shear band is weaker for systems of disks, which also do not exhibit meta-stable states. The slow relaxation of velocity profiles and local densities for ellipses are coupled to logarithmically slow evolution in the local orientational order parameter of ellipses in the compacted region far from the shear band. This reorientation of particles incrementally increases the packing fraction far from the inner wheel, and allows the system to dilate more in the inner region where the shear band is located. The anomalous rate dependence seen for ellipses is therefore tied to the orientational degree of freedom. Although logarithmic rate dependence has been observed for spherical/circular particles, ellipses show much stronger rate dependence for stress fluctuations.

The present experiments suggest that, more generally, when the density is coupled to another system property,

there exists the possibility of a long internal response time as the system responds to shear or other strains by forming more compact structures. We note that complex grain shapes do not have any obvious orientational order. But, they do have the property that rotations of the grains can lead to changes of density or stresses. These changes might be either positive or negative, depending on the initial conditions and the strain history.

We thank Dr. Joshua Dijksman for helping with setting up these experiments, and we very much appreciate discussions with Prof. Karin Dahmen. This work was supported by NSF grants DMR-0906908, DMR-1206351, and ARO grant W911NF-11-1-0110.

-
- [1] C. S. O’Hern, L. E. Silbert, A. J. Liu, S. A. Langer, Phys. Rev. E **68** 011306 (2003).
 - [2] M. van Hecke, J. Phys. Condens. Matter **22**, 033101 (2010).
 - [3] D. Bi, J. Zhang, B. Chakraborty, R.P. Behringer, Nature **480**, 355358 (2011).
 - [4] C. Heussinger, J. L. Barrat, Phys. Rev. Lett. **102**, 218303 (2009).
 - [5] P. Olsson, S. Teitel, Phys. Rev. E **83**, 030302(R) (2011).
 - [6] D. Howell, R. P. Behringer, C. Veje, Phys. Rev. Lett. **82**, 52415244 (1999).
 - [7] B. Miller, C. O’Hern, R. P. Behringer, Phys. Rev. Lett. **77**, 31103113 (1996).
 - [8] R. R. Hartley, R. P. Behringer, Nature **421**, 928-931 (2003).
 - [9] R. P. Behringer, D. Bi, B. Chakraborty, S. Henkes, R. R. Hartley, PRL **101**, 268301 (2008).
 - [10] J.A. Dijksman, G.H. Wortel, L.T.H. van Dellen, O. Dauchot, M. van Hecke, Phys. Rev. Lett. **107**, 108303 (2011).
 - [11] P. Schall, M. van Hecke, Annu. Rev. Fluid Mech. **42**, 67-88 (2010).
 - [12] J. Geng, G. Reydellet, E. Clément, R.P. Behringer, Physica D **182**, 274303 (2003).
 - [13] J. Geng, R.P. Behringer, Phys. Rev. E **71**, 011302 (2005).
 - [14] C. Marone, C. B. Raleigh, C.H.J. Scholz, Geophysical Research **95**, 7007 (1990).
 - [15] M. Otsuki, H. Hayakawa, Phys. Rev. E **83**, 051301 (2011).
 - [16] J. T. Jenkins and S. B. Savage, J. Fluid Mech. **130**, 187-202 (1983).
 - [17] K. A. Reddy, Y. Forterre, O. Pouliquen, Phys. Rev. Lett. **106**, 108301 (2011).
 - [18] M. Mailman, C. F. Schreck, C. O’Hern, B. Chakraborty, Phys. Rev. Lett. **102**, 255501 (2009).
 - [19] A. Donev, I. Cisse, D. Sachs, E. A. Variano, Fr. H. Stillinger, R. Connelly, S. Torquato, P. M. Chaikin, Science, **303** 990 (2004).
 - [20] K. A. Dahmen, Y. Ben-Zion, J. T. Uhl, Nature Physics **7**, 554557 (2011).
 - [21] P. M. Chaikin, T. C. Lubensky, *Principles of Condensed Matter Physics*, Cambridge University Press, (1995).
 - [22] Supplementary material 1 (video of particle motion)
 - [23] Supplementary material 2 (video of photoelastic response)
 - [24] S. Farhadi, Shape Effects on Jamming of Granular Mate-

rials, Ph.D. Thesis, Duke University, 2012 (unpublished).